Multipactor susceptibility on a dielectric with two carrier frequencies

Asif Iqbal,[1] John Verboncoeur,[1,2] and Peng Zhang[1,a)]
[1]Department of Electrical and Computer Engineering, Michigan State University, East Lansing, Michigan 48824-1226, USA
[2]Department of Computational Mathematics, Science and Engineering, Michigan State University, East Lansing, Michigan 48824, USA

(Received 31 January 2018; accepted 12 March 2018; published online 29 March 2018)

This work investigates multipactor discharge on a single dielectric surface with two carrier frequencies of an rf electric field. We use Monte Carlo simulations and analytical calculations to obtain susceptibility diagrams in terms of the rf electric field and normal electric field due to the residual charge on the dielectric. It is found that in contrast to the single frequency case, in general, the presence of a second carrier frequency of the rf electric field increases the threshold of the magnitude of the rf electric field to initiate multipactor. The effects of the relative strength and phase, and the frequency separation of the two carrier frequencies are examined. The conditions to minimize mulitpactor are derived. *Published by AIP Publishing.* https://doi.org/10.1063/1.5024365

I. INTRODUCTION

Multipactor[1–7] is a nonlinear phenomenon in which an electron avalanche driven by a high frequency rf field sustains itself by an exponential charge growth through secondary electron emission from a metallic or dielectric surface. If this avalanche of electrons reaches a sufficiently high saturation level[2,3,5] by inducing appreciable outgassing from the surface, it can eventually turn into a gaseous-like discharge within the desorbed gas layer which is sometimes called flashover and may cause breakdown of dielectric windows,[8–10] erosion of metallic structures, melting of internal components, and perforation of vacuum walls.[2] Hence, avoiding multipactor has been a major concern for high power microwave (HPM) sources, rf accelerators,[10] and space-based communication systems.[11]

Multicarrier operation is a common feature in many modern systems[12] in which a number of carrier waves are transmitted simultaneously at different frequencies through the system. Incidental superposition of multiple frequencies can also occur in many rf components due to coupling between imperfectly isolated subsystems, such as in transmission lines and supporting components. Several studies have been carried out on the phenomenon of multipactor for multicarrier operations in parallel plate geometry.[12–16] Semenov *et al.* showed[12] that exposure of a simple one-dimensional metallic gap to a homogeneous rf field consisting of two carrier waves with close but separated frequencies leads to a suppression of multipactor breakdown, if appropriate combinations of carrier amplitudes and frequency separation are chosen. Semi-empirical multicarrier multipaction threshold prediction methods[17] have been adopted in the industry including the widely employed "20 gap crossing rule" which is based on the dependency of the multipactor discharge on the signal envelope, stating that multipactor occurs when the multi-carrier signal envelope exceeds the single carrier multipactor threshold for an interval equal to or higher than 20 times the time for an electron to cross the gap.[17] Anza *et al.* investigated the nonstationary statistical theory[15] of multipactor prediction in parallel plate geometries for multicarrier signals by particle in cell (PIC) simulations[13] and experimental validation.[16] Rice and Verboncoeur examined[14] multipactor trajectories in parallel plate geometry with perturbative second, third, and fourth harmonic modes. Investigations reveal that multicarrier operation results in a modulation of the signal amplitude, significantly modifying the conditions for the development of multipactor, and can be employed as a multipactor suppression technique for parallel plate systems. However, to the author's knowledge, the existing literature does not offer a comprehensive analysis or estimation of such modification introduced in the single surface geometry.

The theory of multipactor discharge on a single dielectric surface resulting from an rf field with single frequency has been extensively researched, including Monte Carlo (MC) particle simulations,[4] particle-in-cell (PIC) simulations,[18,19] analytical calculations,[4] dynamic theory,[20] and statistical theory.[21] The effects of space charge,[22–24] external electric and magnetic fields,[5,22,25,26] oblique rf electric fields,[27] wave reflection,[25] and desorption or background gases[5,23] have been investigated. The transition of window breakdown from vacuum multipactor discharge to rf plasma has been studied, by both PIC simulations[18] and volume-averaged global models (GM).[26,28] Analytical scaling laws have been derived for dielectric window breakdown in vacuum and collisional regimes.[29]

In this paper, we model multipactor discharge on single dielectric surface with an rf signal consisting of two carrier frequencies. This additional carrier frequency is expected to increase the threshold of the rf electric field for multipactor initiation and also suppress multipactor, with appropriate choices for its relative strength and phase relative to the fundamental mode, as inferred from several investigations on multipactor in parallel plate geometry.[12–14] Here, we use MC simulations and analytical calculations to determine the condition for the onset of multipactor discharge at various combinations of the frequency separation, relative strength, and

a)Author to whom correspondence should be addressed: pz@egr.msu.edu

relative phase between the two carrier frequencies of the rf electric field.

II. MONTE CARLO MODEL AND ANALYTICAL THEORY

The multipactor electrons are subjected to forces imposed by the normal electric field E_{dc} acting along the x-direction and the rf electric field $[E_{rf}\sin(\omega t+\theta)+\beta E_{rf}\sin(n\omega t+\theta+\gamma)]$ acting along the y-direction (Fig. 1). Here, E_{rf} is the peak electric field strength, ω is the radian frequency, and θ is the field starting phase, of the fundamental carrier mode. β is the field strength of the second carrier mode relative to the fundamental mode, n is the ratio of the two carrier frequencies, and γ is the relative phase of the second carrier mode. Here, n need not be an integer. The possible space-charge effects due to multipactor electrons[18,22,23,30] are not considered beyond the varying strength of E_{dc}. Referring to Fig. 1, the flight trajectory of a multipactor electron is governed by the force law

$$m\frac{\partial\vec{v}}{\partial t}=-|e|\left[\vec{E}_{rf}\sin(\omega t+\theta)+\beta\vec{E}_{rf}\sin(n\omega t+\theta+\gamma)+\vec{E}_{dc}\right]. \tag{1}$$

From this, we obtain

$$v_x=-\frac{|e|}{m}E_{dc}t+v_0\sin\phi, \tag{2a}$$

$$v_y=\frac{|e|}{m\omega}E_{rf}\left\{\cos(\omega t+\theta)-\cos\theta+\frac{\beta}{n}[\cos(n\omega t+\theta+\gamma)-\cos(\theta+\gamma)]\right\}+v_0\cos\phi, \tag{2b}$$

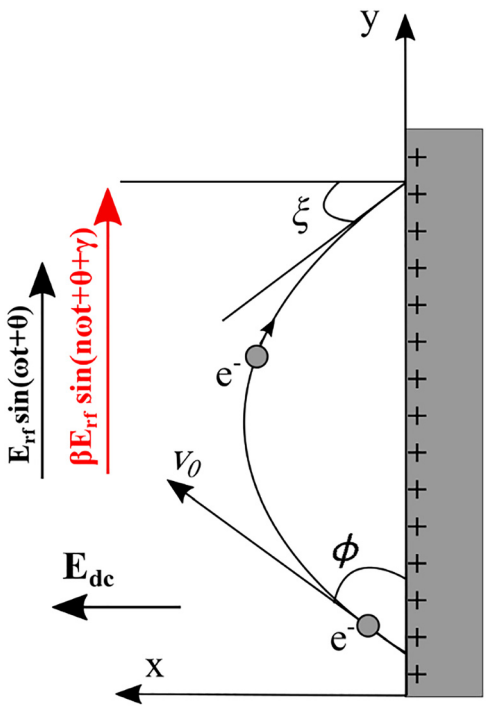

FIG. 1. Schematic of a single-surface multipactor in a normal electric field and a parallel rf field with two carrier frequencies.

where the last terms account for the emission velocity at $t=0$. From Eq. (2), the transit time of an electron in flight is given by

$$\tau=\frac{2mv_0\sin\phi}{|e|E_{dc}}. \tag{3}$$

The average number of secondary electrons produced by the impact of each primary electron upon the surface, called the secondary electron yield, δ, is a function of the impact energy of the primary electron, E_i, and the angle to the normal, ξ, at which it strikes the surface.[31] It also depends on material properties translating into two parameters, the maximum yield, δ_{max}, and the energy at which it occurs, E_{max}. We specify these parameters and adopt Vaughan's empirical formula,[31] to estimate the secondary electron yield for normal incidence

$$\delta=\delta(E_i)\cong\delta_{max}(we^{1-w})^k, \tag{4}$$

where $w=E_i/E_{max}$ and $k=0.62$ for $w<1$ and $k=0.25$ for $w=1$. Two values of impact energy, termed the first and second crossover points, E_1 and E_2, respectively, result in a yield of 1, with $\delta>1$ in between. The parameters are adjusted in calculating the yield, for impact at an angle ξ with respect to the normal (Fig. 1), according to the following equations:[31,32]

$$E_{max}=E_{max0}\left(1+\frac{K_{sE}\xi^2}{2\pi}\right), \tag{5a}$$

$$\delta_{max}=\delta_{max0}\left(1+\frac{K_{s\delta}\xi^2}{2\pi}\right). \tag{5b}$$

Here, E_{max0} and δ_{max0} are the parameters for an impact angle $\xi=0$ (i.e., normal to the surface, cf. Fig. 1), and k_{sE} and $k_{s\delta}$ are surface smoothness factors for E and δ ranging from 0 for a rough surface to 2 for a polished surface. In this paper, we set the values $k_{sE}=k_{s\delta}=1$, representing a typical dull surface.[31,32] It is worth noting that in this situation, since the electrons gain their energy from the parallel rf field, most impacts will be at almost grazing incidence ($\xi\approx\pi/2$).

To calculate the growth rate of the multipactor discharge, we follow the trajectory of a weighted macroparticle over a large number of impacts in a MC simulation.[4,5,20] The initial rf phase, θ, is uniformly distributed over $0<\theta<2\pi$ (Fig. 1). Each time a macroparticle leaves the surface, we assign it a random initial energy $E_0=(1/2)mv_0^2$ and angle ϕ according to the following distributions:[4]

$$f(E_0)=\frac{E_0}{E_{0m}^2}e^{-\left(\frac{E_0}{E_{0m}}\right)}, \tag{6a}$$

$$g(\phi)=\frac{1}{2}\sin\phi, \tag{6b}$$

where E_{0m} is the peak of the distribution of emission energies, on the order of the work function, i.e., a few eV.[2,4,20] The expected value of E_0 is $2E_{0m}$, and $\int g(\phi)d\phi=1$ over $0<\phi<\pi$. Substituting these random values of initial velocity and angle into Eqs. (2) and (3), we obtain the impact

energy, E_i, and impact angle, ξ, and hence, the secondary electron yield, δ, from Eq. (4). We use this value of the yield to adjust the charge and mass on the macroparticle and then emit it again with a random velocity. We repeat the process to obtain a series of yields $(\delta_1.\delta_2\ldots\delta_N)$ for a large number of impacts. In order to average out the dependence of a secondary electron's flight trajectory upon the rf conditions of a primary electron's impact onto the surface, the phase of the rf field θ can be randomly assigned at the beginning of each flight. Alternatively, the rf phase θ is randomly assigned only initially and then calculated self-consistently $(\theta_{i+1} = \theta_i + \omega\tau_i)$ at the beginning of each flight for a given macroparticle, the process of which is then repeated for many independent macroparticles. It is found that the two approaches yield very similar results in terms of multipactor susceptibility. In this paper, we present the results using the latter method. The average value of secondary yield over N impacts is then calculated as $\bar{\delta} = (\delta_1.\delta_2.....\delta_N)^{1/N}$, where a large N (e.g. = 200) is used in the calculation. The simulation is then repeated for $M = 100$ (independent) macroparticles. The median value of the secondary yield of these M independent macroparticles is calculated, which represents either an exponentially growing ($\bar{\delta} > 1$) or an exponentially decaying ($\bar{\delta} < 1$) trend in the number of electrons in the avalanche. This trend depends on the external parameters, such as E_{dc}, E_{rf}, δ_{max0}, θ, n, β, and γ. For any given values of the fields, this average value of the secondary electron yield averaged over the distributions of random emission energy, emission angle, and rf phase at emission, gives the growth rate. The boundaries of the multipactor susceptibility are determined when the exponential growth rate of the electrons equals zero. Figure 2 shows the susceptibility diagram for the multipactor boundaries with only the fundamental carrier

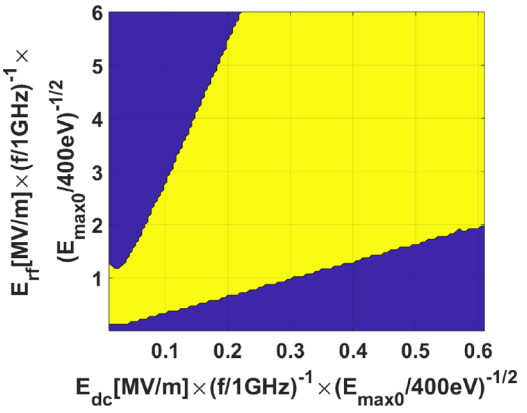

FIG. 2. Multipactor susceptibility boundaries (yellow regions are subject to multipactor susceptibility) with single carrier frequency of the rf field, from Monte Carlo simulation, in the (E_{dc}, E_{rf}) plane for $\delta_{max0} = 3$, $E_{0m}/E_{max0} = 0.005$. Here, E_{rf} is the amplitude of the tangential rf electric field at frequency f, E_{dc} is the normal electric field on the dielectric surface, δ_{max0} is the maximum secondary electron yield occurring at impact energy E_{max0}, and $2E_{0m}$ is the average emission energy of secondary electrons.

frequency of the rf field, ω. Roughly, the lower (upper) boundary corresponds to electron impact energy on the dielectric surface equal to the first (second) crossover point in the secondary electron yield curve[33] and multipactor saturation typically occurs at the lower boundary.

In order to construct simple analytical solutions for the susceptibility diagrams, we follow Ref. 3 and assume that all electrons are emitted normal to the surface (i.e., $\phi = 90°$ in Fig. 1), with a single energy $E_0 = (1/2)mv_0^2 = 2E_{0m}$. Hence, substituting $\phi = 90°$ into Eqs. (2)–(4), averaging over rf phase θ, and setting the resulting average impact energy equal to E_1 and E_2 at $\xi \approx \pi/2$ [cf. Eqs. (4) and (5)], we obtain the following normalized equations for the lower and upper boundaries:

$$\bar{E}_{rf1,2} = \sqrt{\frac{2\bar{E}_{1,2}}{1 - \cos\bar{\tau} + \frac{\beta^2}{n^2}(1 - \cos n\bar{\tau}) + \frac{\beta}{n}[\cos(n\bar{\tau} - \bar{\tau} + \gamma) - \cos(\bar{\tau} - \gamma) - \cos(n\bar{\tau} + \gamma) + \cos\gamma]}}, \tag{7}$$

where $\bar{E}_{rf1,2} = \frac{|e|E_{rf1,2}}{\omega\sqrt{mE_{max0}}}$, $\bar{E}_{1,2} = \frac{E_{1,2}}{E_{max0}}$, $\bar{\tau} = \frac{2\sqrt{2\bar{E}_0}}{\bar{E}_{dc}}$, $\bar{E}_0 = \frac{E_0}{E_{max0}}$, and $\bar{E}_{dc} = \frac{|e|E_{dc}}{\omega\sqrt{mE_{max0}}}$. When $\beta = 0$, Eq. (7) recovers the boundaries of multipactor susceptibility for a single frequency rf field only.[3,4]

In the limit of large normal electric field, $\bar{E}_{dc} \gg 1$, or equivalently, $\bar{\tau} \to 0$, with the approximations $\sin\bar{\tau} \approx \bar{\tau}$ and $\cos\bar{\tau} \approx (1 - \bar{\tau}^2/2)$, Eq. (7) reduces to

$$\bar{E}_{rf1,2} = K\bar{E}_{dc}, \tag{8}$$

establishing a linear relationship between $\bar{E}_{rf}$ and $\bar{E}_{dc}$, with the slope

$$K = \frac{1}{2}\sqrt{\frac{\frac{\bar{E}_{1,2}}{\bar{E}_0}}{\frac{\beta^2}{2} + \beta\cos\gamma + \frac{1}{2}}}. \tag{9}$$

III. RESULTS

Figure 3 shows the susceptibility boundaries when a second carrier frequency of the rf field, $n\omega$, is introduced with a relative rf field strength of β and a relative phase of γ to the fundamental mode. The presence of a second carrier frequency significantly changes the susceptibility boundaries depending upon the values of β and γ. As we introduce the second carrier frequency with the same phase of the fundamental mode, i.e., $\gamma = 0$, the magnitude of the rf field required to initiate multipactor for a given normal electric field decreases, as compared to Fig. 2. For a given β, as γ increases, both the lower and upper mutipactor susceptibility boundaries increase, thus decreasing the "area" of the multipactor susceptibility in the (E_{rf}, E_{dc}) plane in which multipactor would occur.[4,20] The two boundaries reach a maximum value around $\gamma \sim \pi$ and then decrease as γ approaches 2π. As the relative strength β of the second

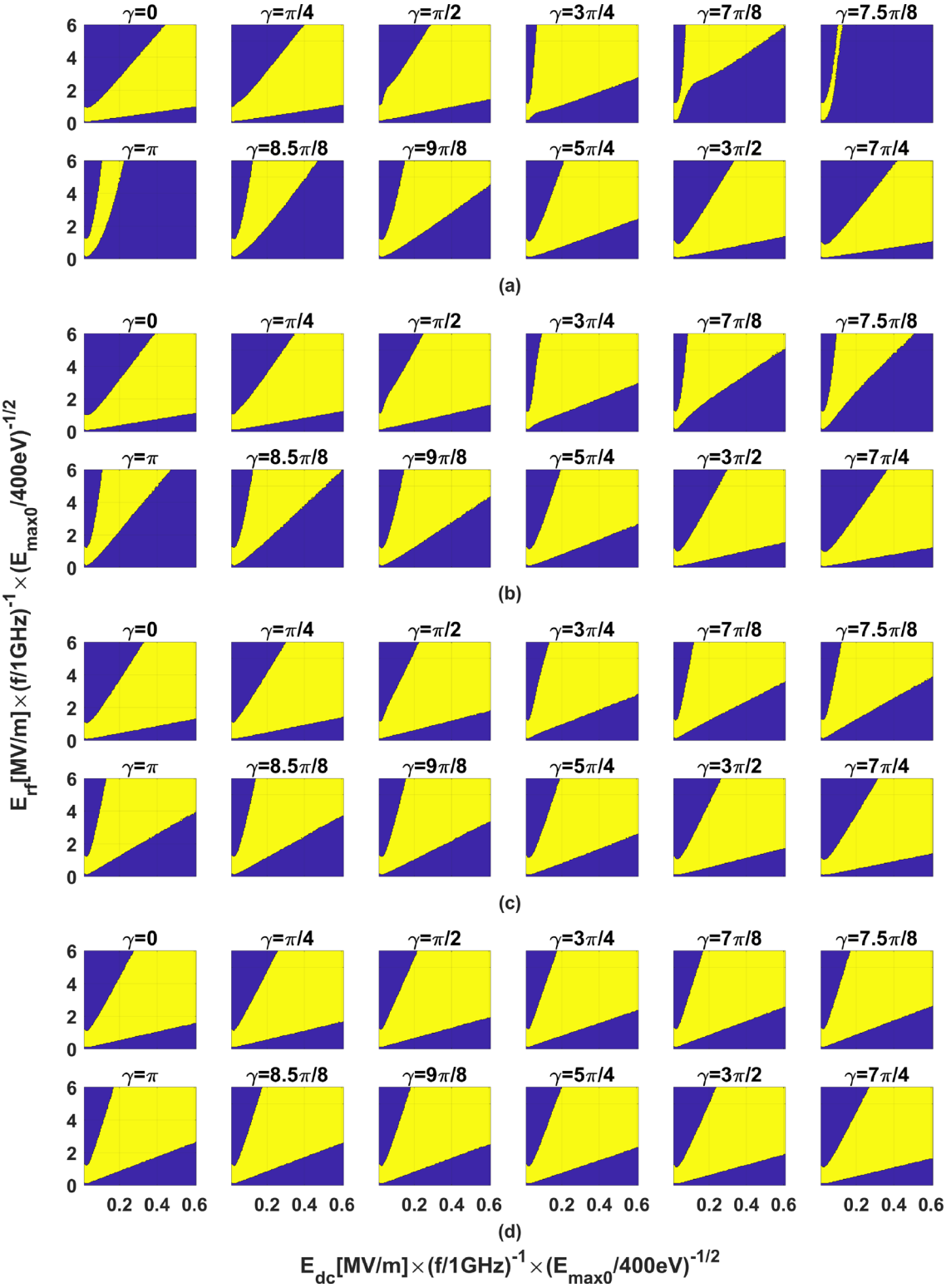

FIG. 3. Multipactor susceptibility boundaries with two carrier frequencies of the rf field, from Monte Carlo simulation, in the (E_{dc}, E_{rf}) plane for $\delta_{max0} = 3$, $E_{0m}/E_{max0} = 0.005$, relative frequency of the second carrier, $n = 2$, and relative phase between the two carriers, $\gamma = 0, \frac{\pi}{4}, \frac{\pi}{2}, \frac{3\pi}{4}, \frac{7\pi}{8}, \frac{7.5\pi}{8}$, $\pi, \frac{8.5\pi}{8}, \frac{9\pi}{8}, \frac{5\pi}{4}, \frac{3\pi}{2}$, and $\frac{7\pi}{4}$, for the relative strength of the second carrier (a) $\beta = 1$, (b) $\beta = 0.75$, (c) $\beta = 0.5$, and (d) $\beta = 0.25$.

frequency carrier decreases from Figs. 3(a)–3(d), its effects on the multipactor susceptibility become less pronounced. We note that when β is very small ($\sim$0), the second frequency carrier has little effect on the multipactor susceptibility.

The modification of multipactor susceptibility boundaries introduced by the addition of the second carrier mode can be attributed to the modulation of the rf signal amplitude that periodically varies over the relative phase between the two carriers, which in turn distorts the electron trajectory,

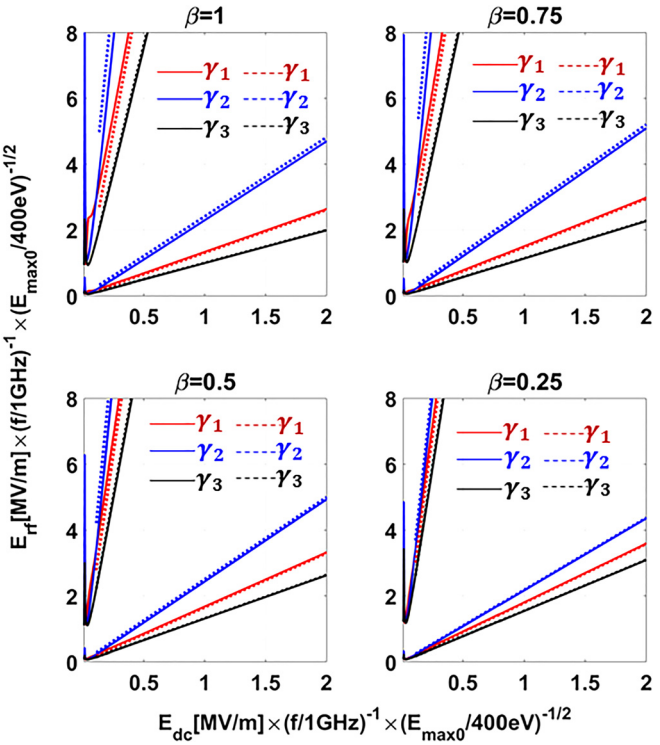

FIG. 4. Multipactor susceptibility boundaries with two carrier frequencies of the rf field, from direct calculation of Eq. (7) (solid lines), and linear approximation of Eq. (8) (broken lines), in the (E_{dc}, E_{rf}) plane for $\delta_{max0} = 3$, $E_{0m}/E_{max0} = 0.005$, relative frequency of the second carrier, $n = 2$, relative phase between the two carriers, $\gamma_1 = \pi/2$, $\gamma_2 = 5\pi/4$, $\gamma_3 = 7\pi/4$, and relative strength of the second carrier, $\beta = 1$, 0.75, 0.5, and 0.25.

leading to a modified impact energy and angle, and therefore a different secondary electron yield.

Figure 4 shows the multipactor region boundaries calculated from Eqs. (7) (solid lines) and (8) (broken lines). The drastic simplification introduced to derive Eqs. (7)–(9) does not qualitatively change the solution shown in Fig. 3. These equations may be used to choose the optimum operating conditions for specific E_{rf} windows.

Both the MC simulations and the analytical theory show that the multipactor susceptibility boundaries depend strongly on the relative phase of the second carrier frequency, γ. From Eq. (9), it can be easily shown that, for a given β, the maximum slope of $\bar{E}_{rf}$ is

$$K(\gamma)_{max} = \frac{1}{(1-\beta)}\sqrt{\frac{\bar{E}_{1,2}}{2\bar{E}_0}}, \tag{10}$$

which occurs at $\gamma = \pi$; and the minimum slope of $\bar{E}_{rf}$ is

$$K(\gamma)_{min} = \frac{1}{(1+\beta)}\sqrt{\frac{\bar{E}_{1,2}}{2\bar{E}_0}}, \tag{11}$$

which occurs at $\gamma = 0$ and 2π. Note that when $\beta = 1$, Eq. (10) gives $K(\gamma = \pi)_{max} = \infty$, indicating complete multipactor suppression under the simplified assumptions to derive Eqs. (7)–(10). However, MC simulations [Fig. 3(a)] show that multipactor can only be minimized near $\gamma \approx \pi$. In Fig. 5, the dE_{rf}/dE_{dc} curves for the upper and the lower boundaries calculated from Eq. (9) are plotted against γ for different values of β. The results are consistent with Figs. 3 and 4. For low power operations of $\bar{E}_{rf}$, it would be desirable to maximize the slope of the lower susceptibility boundary to minimize the "area"[5] of the multipactor susceptibility in the (E_{rf}, E_{dc}) plane in which multipactor would occur. Similarly, for operations where $\bar{E}_{rf}$ is sufficiently large so that the upper boundary becomes significant, it would be desirable to minimize the slope of the upper susceptibility boundary, essentially minimizing the "area" of the multipactor susceptibility in the (E_{rf}, E_{dc}) plane.

Figure 6 shows slopes dE_{rf}/dE_{dc} for the lower and the upper boundaries calculated from Eq. (9) plotted against β. For $\gamma < \pi/2$ or $\gamma > 3\pi/2$, the slopes for both the lower and upper boundaries decrease as β increases. For $\pi/2 < \gamma < 3\pi/2$, the slopes of both boundaries increase with β and then decrease as $\beta \to 1$. The results are consistent with those in Figs. 3 and 4. The maximum slope of the susceptibility boundaries occurs at $\beta = -\cos\gamma$ for $\pi/2 < \gamma < 3\pi/2$, which is given as

$$K(\beta)_{max} = \frac{1}{2}\sqrt{\frac{\frac{\bar{E}_{1,2}}{\bar{E}_0}}{\frac{1}{2}\left(1-\cos^2\gamma\right)}}, \tag{12}$$

which is also shown in Fig. 6.

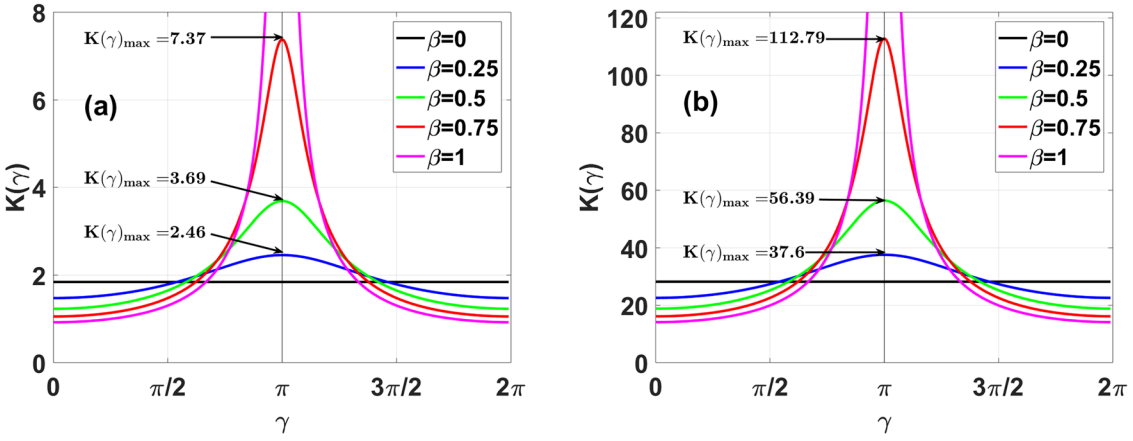

FIG. 5. Slopes of (a) the lower and (b) the upper susceptibility boundaries as a function of the relative phase between the two carriers, γ, from Eq. (10), for $\delta_{max0} = 3$, $E_{0m}/E_{max0} = 0.005$, relative strength of the second carrier, $\beta = 0$, 0.25, 0.5, 0.75, and 1. Also shown are the maximum slope of both boundaries from Eq. (10) at $\gamma = \pi$.

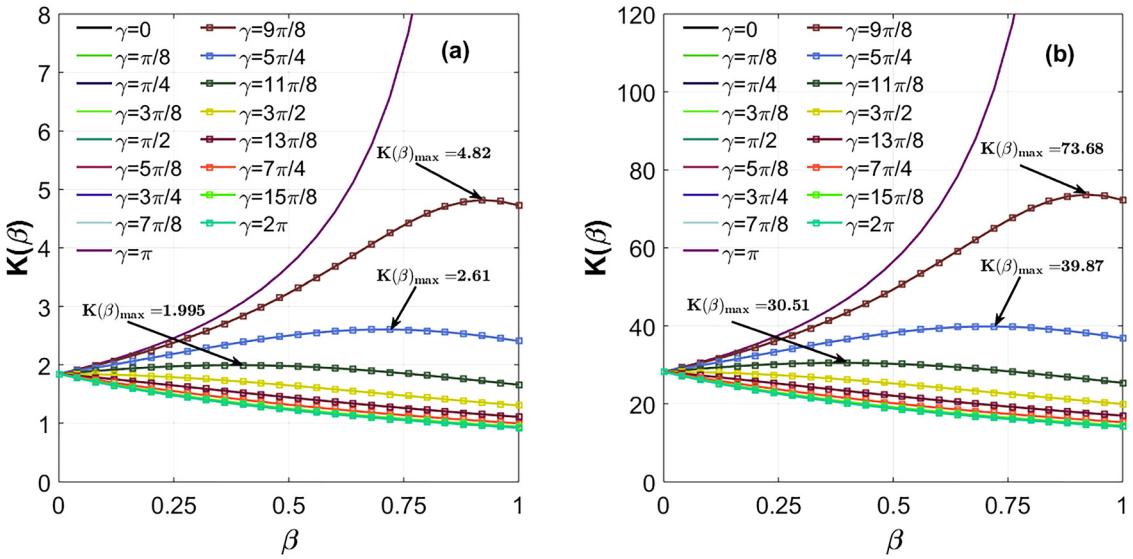

FIG. 6. Slopes of (a) the lower and (b) the upper susceptibility boundaries vs relative strength of the second carrier, β, from Eq. (9), for $\delta_{max0} = 3$, $E_{0m}/E_{max0} = 0.005$, and the relative phase between the two carriers, $\gamma = 0$ to 2π. Note that the curves corresponding to the relative phase γ and the curves corresponding to the relative phase $(2\pi - \gamma)$ overlap identically. Also shown are the maximum slope of both boundaries occurring at $\beta = -\cos\gamma$, for $\pi/2 < \gamma < 3\pi/2$, given by Eq. (12).

The effects of frequency separation are also examined. Figure 7 shows the lower multipactor susceptibility boundary E_{rf1} as a function of the frequency ratio n, obtained by both MC simulations and analytical calculations from Eq. (7). These solutions demonstrate that $E_{rf1,2}$ is not sensitive to the frequency ratio for a constant normal electric field. For any particular value of E_{dc}, the rf field required to initiate multipactor is significantly increased by the addition of the second carrier frequency with a relative phase $\gamma = \pi$. This increase is observed over almost the entire practical range of relative frequencies of the second carrier, $1 < n < 3$.

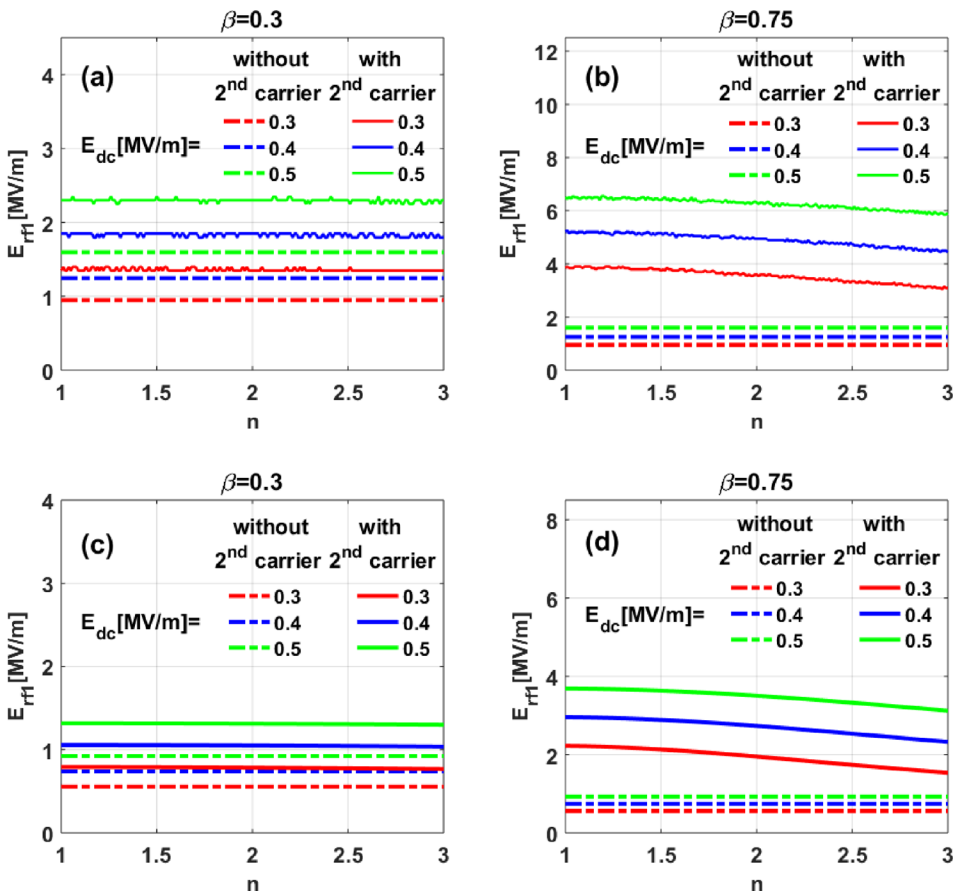

FIG. 7. Lower rf field boundary for multipactor initiation, E_{rf1}, as a function of the frequency ratio, n from Monte Carlo simulations for (a) $\beta = 0.3$, (b) $\beta = 0.75$, and from Eq. (7) for (c) $\beta = 0.3$, and (d) $\beta = 0.75$. In the calculation, we use $\delta_{max0} = 3$, $E_{0m}/E_{max0} = 0.005$, and relative phase of the second carrier, $\gamma = \pi$.

IV. CONCLUDING REMARKS

This work presents a study of multipactor breakdown in single dielectric surfaces exposed to an rf field with two-carrier frequencies. The study was carried out using both numerical simulations and analytical calculations. We found that the presence of a second carrier frequency in the rf electric field can increase the magnitude of rf electric field threshold to initiate multipactor. The effects of the relative strength β and relative phase γ, and the frequency separation of the two carrier frequencies are examined in detail. The multipactor susceptibility boundaries depend strongly on the relative strength β and relative phase γ, but are insensitive to the frequency ratio n between the two carrier frequencies. The conditions to minimize mulitpactor are derived. For a given relative field strength β, both the lower and upper multipactor thresholds are maximized (corresponding boundaries have the maximum slope) when the relative phase $\gamma \rightarrow \pi$, and minimized (corresponding boundaries have the minimum slope) when $\gamma \rightarrow 0$ (or 2π).

Our results show that single-surface multipactor suppression by dual frequency operation can be obtained only when the magnitude of the second carrier is comparable to that of the fundamental carrier (i.e., $\beta > 0.25$). Compared to 2-surface multipactor in parallel plate systems constrained by the resonant conditions,[12] generally single-surface multipactor is more likely to occur. Thus, it seems that the suppression of single surface multipactor with dual frequency operation is more difficult than that of 2-surface multipactor. A conclusive comment on this requires a detailed analysis of the time dependent physics, which is a subject of our ongoing study.

Further studies may include the effects of both amplitude and frequency modulation of the rf fields, multi-carrier (more than two frequencies) operation, space charge, the dynamics of the normal electric field to the dielectric surface E_{dc}, and the connection to two-surface multipactor.

ACKNOWLEDGMENTS

The authors would like to thank useful discussions with Dr. Y. Y. Lau, Dr. Scott Rice, Dr. Rami Kishek, and Dr. John Luginsland. This work was supported by AFOSR MURI Grant No. FA9550-18-1-0062 and an MSU Foundation Strategic Partnership Grant.

[1]P. T. Farnsworth, J. Franklin Inst. **218**, 411 (1934).
[2]J. R. M. Vaughan, IEEE Trans. Electron Devices **35**, 1172 (1988).
[3]R. A. Kishek and Y. Y. Lau, Phys. Rev. Lett. **80**, 193 (1998).
[4]R. A. Kishek, Y. Y. Lau, L. K. Ang, A. Valfells, and R. M. Gilgenbach, Phys. Plasmas **5**, 2120 (1998).
[5]P. Zhang, Y. Y. Lau, M. Franzi, and R. M. Gilgenbach, Phys. Plasmas **18**, 053508 (2011).
[6]A. J. Hatch and H. B. Williams, J. Appl. Phys. **25**, 417 (1954).
[7]A. J. Hatch and H. B. Williams, Phys. Rev. **112**, 681 (1958).
[8]D. H. Preist and R. C. Talcott, IRE Trans. Electron Devices **8**, 243 (1961).
[9]J. R. M. Vaughan, IRE Trans. Electron Devices **8**, 302 (1961).
[10]S. Yamaguchi, S. Michizono, and S. Anami, IEEE Trans. Nucl. Sci. **39**, 278 (1992).
[11]N. Rozario, H. F. Lenzing, K. F. Reardon, M. S. Zarro, and C. G. Baran, IEEE Trans. Microwave Theory Tech. **42**, 558 (1994).
[12]V. Semenov, A. Kryazhev, D. Anderson, and M. Lisak, Phys. Plasmas **8**, 5034 (2001).
[13]S. Anza, M. Mattes, C. Vicente, J. Gil, D. Raboso, V. E. Boria, and B. Gimeno, Phys. Plasmas **18**, 032105 (2011).
[14]S. A. Rice and J. P. Verboncoeur, IEEE Trans. Plasma Sci. **45**, 1739 (2017).
[15]S. Anza, C. Vicente, J. Gil, V. E. Boria, B. Gimeno, and D. Raboso, Phys. Plasmas **17**, 062110 (2010).
[16]S. Anza, C. Vicente, J. Gil, V. E. Boria, and D. Raboso, in *2016 46th European Microwave Conference (EuMC)* (IEEE, 2016), pp. 226–229.
[17]*Space Engineering: Multipacting Design and Test*, edited by ESA-ESTEC (ESA Publication Division, The Netherlands, 2013), Vol. ECSS-20-01A.
[18]H. C. Kim and J. P. Verboncoeur, Phys. Plasmas **13**, 123506 (2006).
[19]H. C. Kim, J. P. Verboncoeur, and Y. Y. Lau, IEEE Trans. Dielectr. Electr. Insul. **14**, 774 (2007).
[20]L. K. Ang, Y. Y. Lau, R. A. Kishek, and R. M. Gilgenbach, IEEE Trans. Plasma Sci. **26**, 290 (1998).
[21]A. Sazontov, V. Semenov, M. Buyanova, N. Vdovicheva, D. Anderson, M. Lisak, J. Puech, and L. Lapierre, Phys. Plasmas **12**, 093501 (2005).
[22]A. Valfells, L. K. Ang, Y. Y. Lau, and R. M. Gilgenbach, Phys. Plasmas **7**, 750 (2000).
[23]C. Chang, G. Liu, C. Tang, C. Chen, S. Qiu, J. Fang, and Q. Hou, Phys. Plasmas **15**, 093508 (2008).
[24]K. D. Bergeron, J. Appl. Phys. **48**, 3073 (1977).
[25]A. G. Sazontov and V. E. Nevchaev, Phys. Plasmas **17**, 033509 (2010).
[26]S. K. Nam and J. P. Verboncoeur, Appl. Phys. Lett. **92**, 231502 (2008).
[27]A. Valfells, J. P. Verboncoeur, and Y. Y. Lau, IEEE Trans. Plasma Sci. **28**, 529 (2000).
[28]S. K. Nam, C. Lim, and J. P. Verboncoeur, Phys. Plasmas **16**, 023501 (2009).
[29]Y. Y. Lau, J. P. Verboncoeur, and H. C. Kim, Appl. Phys. Lett. **89**, 261501 (2006).
[30]A. Neuber, J. Dickens, D. Hemmert, H. Krompholz, L. L. Hatfield, and M. Kristiansen, IEEE Trans. Plasma Sci. **26**, 296 (1998).
[31]J. R. M. Vaughan, IEEE Trans. Electron Devices **36**, 1963 (1989).
[32]R. M. Vaughan, IEEE Trans. Electron Devices **40**, 830 (1993).
[33]B. W. Hoff, P. J. Mardahl, R. M. Gilgenbach, M. D. Haworth, D. M. French, Y. Y. Lau, and M. Franzi, Rev. Sci. Instrum. **80**, 094702 (2009).